New algorithms for discrete dislocation modeling of fracture

2011 Modelling Simul. Mater. Sci. Eng. 19 045009

(http://iopscience.iop.org/0965-0393/19/4/045009)

Modelling Simul. Mater. Sci. Eng. **19** (2011) 045009 (12pp) doi:10.1088/0965-0393/19/4/045009

New algorithms for discrete dislocation modeling of fracture

Srinath S Chakravarthy and William A Curtin

School of Engineering, Brown University, 182 Hope Street, Providence, RI 02912, USA

Received 22 October 2010, in final form 4 May 2011
Published 24 May 2011
Online at stacks.iop.org/MSMSE/19/045009

Abstract
The application of discrete dislocation (DD) dynamics methods to study materials with realistic yield stresses and realistic cohesive strengths requires new algorithms. Here, limitations of the standard algorithms are discussed, and then new algorithms to overcome these limitations are presented and their successes demonstrated by example. With these new methods, the stability, accuracy and robustness of the DD methodology for the study of deformation and fracture is significantly improved.

(Some figures in this article are in colour only in the electronic version)

1. Introduction

Discrete dislocation (DD) methods have emerged over the last two decades as a means to study plastic deformation at the sub-continuum scale, providing fundamental understanding of strengthening/hardening phenomena and of size effects in plasticity. Fully three-dimensional DD models have been used primarily to study strain hardening due to dislocation forest interactions in nominally homogeneous blocks of material under uniform loading at the largest scales [1–8], individual dislocation/obstacle interactions [9–15], and individual dislocation loop/ crack tip interactions [16] at the smallest scales and most recently tension, compression and bending in micro/nanoscale pillars or beams [17–19]. For solving complex boundary value problems, the use of 2D plane-strain DD models (e.g. [20]) is common due to high computational cost of 3D DD [7, 8, 19, 21–23]. The two-dimensional plane-strain DD method has been used to provide insight into a variety of fracture problems including fatigue crack growth in single crystals [24], crack growth in thin films [25], confined layers [26, 27], bi-material interfaces [28] and recently into size effects in fracture [29].

A common approach to modeling crack growth in both DD and continuum plasticity is through the use of a cohesive zone model as a continuum model of the complex nonlinear separation of atomic planes. The primary properties of a cohesive zone model in realistic material systems are the cohesive strength σ_{coh}, typically 2–20 GPa, and the fracture energy Γ_0, typically a few J m^{-2}. Two characteristic lengths associated with the cohesive zone are

0965-0393/11/045009+12$33.00

the critical opening $\delta_c \sim \Gamma_0/\sigma_{coh}$, typically 0.1 nm and thus comparable to the dislocation Burgers vector, and the critical cohesive length $\delta_{coh} \sim \mu\Gamma_0/\sigma_{coh}^2$, typically 1 nm. Resolving stress and strain fields over the nanometer scale, capturing the interaction of dislocations with a nanoscale cohesive zone, and modeling crack growth over the several micrometers needed to establish the material fracture, present several computational challenges. Existing DD studies of deformation and fracture have thus used idealized material systems with low flow stresses ($\sigma_y \leqslant 100$ MPa) and low cohesive strengths ($\sigma_{coh} \leqslant 1$ GPa) to extract trends in behavior as a function of σ_{coh}/σ_y and other material parameters. It is thus of great interest to extend the capability of the DD method to encompass a broader and more realistic range of material properties.

Here we present several computational enhancements and modifications to algorithms reported in the literature to enable DD modeling of fracture in material systems with realistic cohesive and flow strengths. The paper is organized as follows. In the next section we describe the general framework for DD modeling of deformation and fracture. In sections 3, 4, 5 and 6, we present the details of the existing algorithms, their limitations and new algorithms that overcome these limitations. In section 7 we present an example of the successful implementation of the set of modified algorithms to a system with material properties corresponding to a realistic material. Finally, we present a summary of our enhancements to the DD/CZ methodology.

2. DD formulation

The small strain discrete dislocation dynamics (DD) formulation of [20] treats edge dislocations as line defects with Burgers vector b in a plane strain, isotropic elastic single-crystal material and the changes in geometry due to slip are neglected. The crystal has three slip systems at angles ϕ_α, $\alpha = 1$–3 relative to the x_1-axis. Slip planes on each slip system are introduced with a spacing of d along the x_1-axis. Along each slip plane dislocation sources of strength τ_s and dislocation obstacles of strength τ_{obs} are placed. The areal densities of sources and obstacles are denoted as ρ_s and ρ_{obs}, respectively. Dislocations nucleated from a source on a given slip plane are constrained to glide on that slip plane. Dislocation nucleation from a source occurs when the resolved shear stress on the source exceeds the critical value τ_s for a time period t_{nuc}. The initial separation L_{nuc} of the dipole is chosen such that the dislocation dipole would be in equilibrium under the stress τ_s. Dislocations of opposite sign on the same slip plane are annihilated if they are within a critical distance $L_e = 6b$. Dislocations pinned at obstacles are released when the resolved shear stress exceeds the strength of the obstacle τ_{obs}. The glide motion of dislocations is controlled by a mobility law, where the dislocation velocity glide v is proportional to the Peach–Koehler force (F_{pk}) on the dislocation as $v = F_{pk}/B$ where B is the mobility coefficient. The Peach–Koehler force is $F_{pk} = \tau_{pk}b$, where τ_{pk} is the total resolved shear stress along the glide plane of the dislocation and is composed of contributions from the applied stress, dislocation/dislocation interactions and image stresses due to imposed boundary conditions. To compute τ_{pk}, a superposition method is used wherein total fields are decomposed into the sum of (i) an analytic singular ($\tilde{}$) fields generated by the dislocations in an infinite or semi-infinite space and (ii) a corrective ($\hat{}$) field that accounts for the image forces, the actual problem geometry and the boundary conditions, which is computed using finite elements.

To model fracture, we insert an initial crack into the material described above such that the initial crack tip is at the origin and introduce a cohesive zone model along the crack line ahead of the initial tip and a remote stress intensity (K) field is imposed (see figure 1). The computational strategy is carried out in an incremental manner. At each time step, (i) the

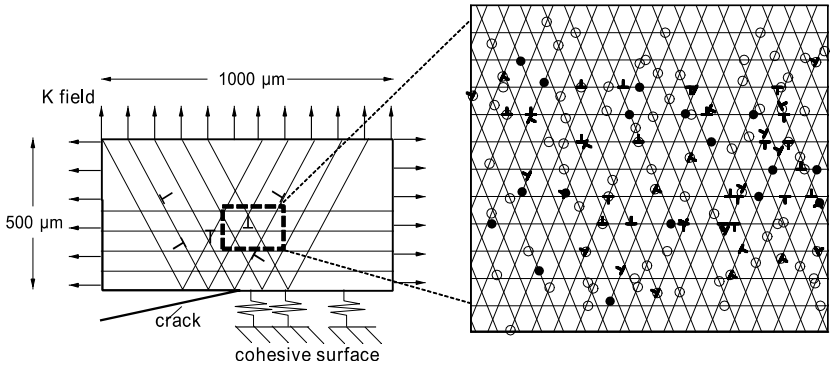

Figure 1. Schematic of the top half of a symmetric DD/CZ fracture simulation geometry. A remote stress intensity loading is applied to a material that deforms via dislocation plasticity and that contains an initial crack and cohesive zone along the line ahead of the crack. The nanoscale material model consists of dislocations, dislocation slip planes, dislocation sources (solid circles) and dislocation obstacles (open circles).

value of the remote K field is increased, (ii) the Peach–Koehler forces $F_{\rm pk}$ on all dislocations are computed, (iii) the dislocation structure is updated by motion of existing dislocations, nucleation of new dislocations, annihilation, pinning at obstacles and dislocations exiting from free surfaces and (iv) the stress and strain state is computed for the updated dislocation structure using the superposition scheme.

In each of the following sections, details of one standard algorithm are described and the shortcomings identified. A new algorithm is then presented that alleviates the shortcomings, as demonstrated by example.

3. Gradient correction to the velocity

The equation of motion for the dislocations along the glide plane is $\mathrm{d}x/\mathrm{d}t = v = F_{\rm pk}/B$. This equation of motion is typically integrated using the forward-Euler method, so that the new position of the dislocation is given by $x(t + \Delta t) = x(t) + v(x(t))\Delta t$. In most DD simulations a maximum time step $\Delta t = 5 \times 10^{-10}$ s has been used along with a maximum dislocation velocity $20\,\mathrm{m\,s^{-1}}$ [24, 30, 31] along with an additional underrelaxation scheme. Segurado *et al* [32] have investigated the effects of the velocity cut-off and the time step showing that the macroscopic uniaxial tensile response and the resulting dislocation structures can be significantly influenced. Furthermore, we have found that when the plastic flow stress is controlled mainly by the obstacles with ensuing pileups, the time step, velocity cut-off and underrelaxation can unduly influence the dislocation unpinning from obstacles. This is easily seen in the simple problem of a dislocation pileup generated by a single source with strength $\tau_{\rm s}$ surrounded by two obstacles with infinite strength at a distance $L_{\rm obs}/2$ on either side of the source (figure 2(*a*)). For an equilibrium pileup of n dislocations, the stress on the pinned dislocation should be n times the applied stress [33]. Figure 2(*b*) shows the stress on the pinned dislocation versus the applied stress as simulated using the standard algorithms. The behavior should be smooth in between successive nucleation events from the source, and show discrete jumps upon each nucleation event. Despite the use of underrelaxation and a velocity cut-off, severe oscillations are observed that arise from incorrect dislocation positions in the pileup stemming from the numerical algorithms. For a time step of 5×10^{-10} s oscillations are observed with as few as three dislocations in the pileup. When the obstacle has a finite

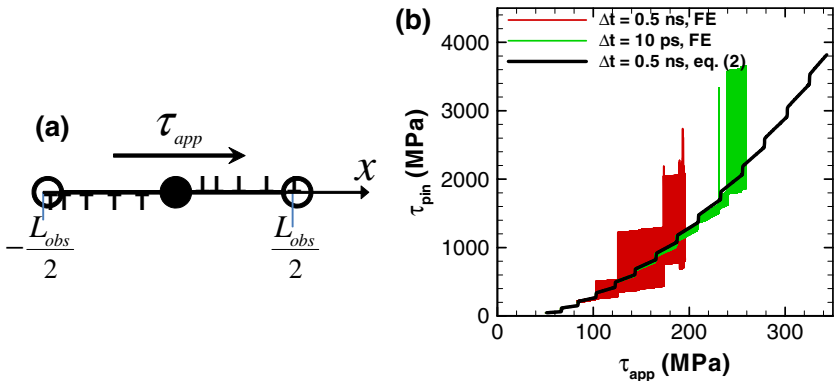

Figure 2. (*a*) Schematic of symmetric pileup problem with source and two equispaced obstacles, (*b*) stress on the pinned dislocation in a symmetric pileup versus applied stress, for a single source with strength $\tau_s = 50$ MPa and obstacle spacing $L_{obs} = 200$ nm. Each step in the curve is associated with the nucleation of a new dislocation dipole. Oscillations with standard forward-Euler method and their elimination using the gradient velocity correction are shown.

strength, these oscillations can cause premature unpinning of a pinned dislocation and lead to a lack of control over the material yield stress. Other artifacts also arise that we will not discuss here.

The problems above stem mainly from rapidly varying stress fields due to closely spaced dislocations, particularly in pileups. The Backward Euler method, given by

$$x(t + \Delta t) = x(t) + v(x(t + \Delta t))\Delta t \tag{1}$$

has higher order accuracy and stability but requires the velocity at the end of the time step, which usually involves an expensive and cumbersome implicit solution process. However, a simple estimate for $v(x(t + \Delta t))$ can be obtained by expanding it in a Taylor series, using the mobility law, and manipulating to solve for the velocity as

$$v(x(t + \Delta t)) = \frac{1}{B}\frac{F_{\rm pk}}{\left(1 - \frac{1}{B}\frac{\partial F_{\rm pk}}{\partial x}\Delta t\right)}. \tag{2}$$

The correction in equation (2) reflects the fact that over the time period Δt the dislocation moves through a spatially varying force field. When the field gradient is large, the correction improves the net dislocation motion in comparison with the forward-Euler scheme, leading to more accurate dislocation positions and avoiding spurious large interaction forces arising when dislocations become too close together due to inaccurate evolution algorithm. Since the dislocation interactions are available as analytical fields, their spatial derivatives are also available in analytical form and the overall computation effort can be easily minimized when the fast multipole method (FMM) is used to accelerate the computation of dislocation interactions (see below). Using the above correction the velocity cut-off is set to $1000\,{\rm m\,s^{-1}}$, which is consistent with the maximum dislocation velocity reported in atomistic simulations [34]. Results for the single pileup problem simulated using the gradient correction show complete elimination of the oscillations (figure 2(*b*)). While some oscillations appear when there are multiple dislocations on multiple slip systems if the time step is too large, a time step of $\Delta t \leqslant 5 \times 10^{-11}$ s eliminates all oscillations and circumvents the need for any additional *ad hoc* underrelaxation algorithms.

4. Dislocation nucleation

In most DD simulations reported to date, a dislocation dipole is instantaneously nucleated at a distance $L_{\text{nuc}}/2$ on each side of the source when the stress on the source has been greater than the nucleation stress τ_{s} for a time period t_{nuc}. For sources located close to the crack plane, the abrupt injection of a dislocation dipole results in a sudden jump in the displacement field on the crack boundary and causes numerical instabilities. In addition, in large pileup situations (strong obstacles) the abrupt injection of the dipole into the existing pileup generates spurious forces on the pileup dislocations inducing oscillations similar to those seen in figure 2(*b*).

To minimize the above problems, we introduce a dipole gradually over the nucleation time t_{nuc} such that the Burgers vector and separation increase linearly with time as

$$b^{\text{dipole}}(t) = b\frac{t}{t_{\text{nuc}}}, \qquad 0 < t \leqslant t_{\text{nuc}}, \quad \tau > \tau_{\text{s}} \tag{3}$$

$$x^{\text{dipole}}(t) = L_{\text{nuc}}\frac{t}{t_{\text{nuc}}}, \qquad 0 < t \leqslant t_{\text{nuc}}, \quad \tau > \tau_{\text{s}}. \tag{4}$$

Equations (3) and (4) ensure that these 'latent' dipoles have the correct Burgers vector and are at the proper nucleation distance when $t = t_{\text{nuc}}$. Algorithmically the 'latent' dislocations are not subjected to the mobility law until $t = t_{\text{nuc}}$, but do contribute to the Peach–Koehler forces on all other dislocations and to the displacements and tractions on the boundaries. If at some time $t_0 < t_{\text{nuc}}$ the stress on the source drops below the nucleation stress, the Burgers vector and position of the dipole are reduced linearly toward zero, i.e. equations (3) and (4) are used with t replaced by $t_0 - t$.

5. Dislocation/cohesive zone (CZ) interactions

For the fracture problem, the cohesive tractions along the crack plane are described by a nonlinear traction-separation ($T - \Delta$) law, where Δ depends on the displacement fields u. In accordance with the standard superposition scheme $\Delta = \hat{\Delta} + \tilde{\Delta}$, the cohesive tractions at the end of an increment are $T^{t+\Delta t} = T(\tilde{\Delta}^{t+\Delta t} + \hat{\Delta}^{t+\Delta t})$. However, during the incremental loading procedure, the updated dislocation fields $\tilde{\Delta}^{t+\Delta t}$ are known and $\hat{\Delta}^{t+\Delta t}$ is the quantity that needs to be solved for. Therefore, expanding $\hat{\Delta}^{t+\Delta t}$ into a Taylor series leads to the linearized traction at the end of the increment as

$$T^{t+\Delta t} = T(\tilde{\Delta}^{t+\Delta t} + \hat{\Delta}^{t}) - K(\tilde{\Delta}^{t+\Delta t} + \hat{\Delta}^{t})\dot{\hat{\Delta}}\Delta t, \tag{5}$$

where $K = \partial T/\partial\Delta$ is a cohesive stiffness, the superscript t indicates time and a superposed dot denotes differentiation in time. The incremental traction $T^{t+\Delta t}$ is then imposed on the boundary, and the finite element solution for $\dot{\hat{\Delta}}$ is obtained from the updated principle of virtual work

$$\int_V \dot{\hat{\sigma}}\delta\epsilon \,\mathrm{d}V + \frac{1}{2}\int_{S_{\text{coh}}} K(\tilde{\Delta}^{t+\Delta t} + \hat{\Delta}^{t})\dot{\hat{\Delta}}\delta\Delta \,\mathrm{d}S = \frac{1}{\Delta t}\left[\int_V \hat{\sigma}^{t}\delta\epsilon \,\mathrm{d}V - \frac{1}{2}\int_{S_{\text{coh}}} T(\tilde{\Delta}^{t+\Delta t} + \hat{\Delta}^{t})\delta\Delta \,\mathrm{d}S\right]. \tag{6}$$

The linearization of the CZ tractions (equation (5)) and the linear incremental solution process (equation (6)) are only valid when the sum $(\tilde{\Delta} + \hat{\Delta})$ is smaller than δ_{c} (the maximum cohesive opening) and Δt is small. When $\tilde{\Delta}^{t+\Delta t} > \delta_{\text{c}}$, the superposition of the dislocation displacement field in (5) causes an initially closed CZ to open. Since the superposed fields

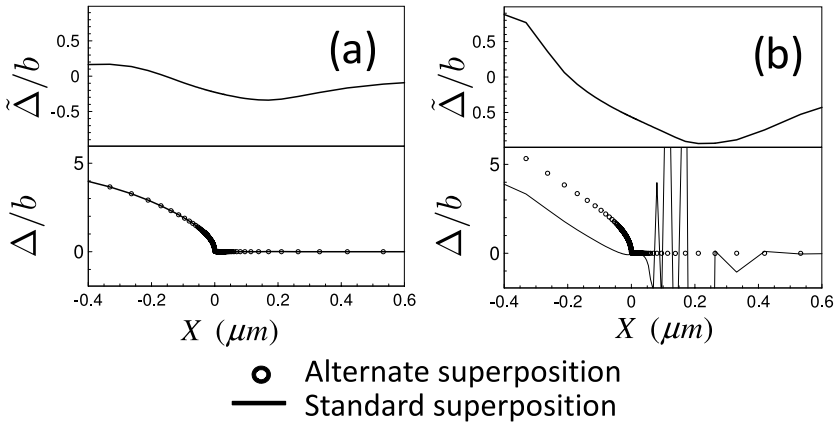

Figure 3. Normalized displacement along the crack line: upper plot shows displacement due to dislocations ($\tilde{\Delta}$); lower plot shows the crack opening profile obtained from FEM solution and DD superposition. (*a*) $\tilde{\Delta} \ll b$, where both superposition schemes are nearly identical and the crack opening is smoothly varying. (*b*) $\tilde{\Delta} \sim b$, where numerical instabilities arise with the standard superposition while the alternative approach remains smooth. Material parameters are $\Gamma_0 = 1.1\,\mathrm{J\,m^{-2}}$, $\sigma_{\mathrm{coh}} = 7\,\mathrm{GPa}$, $\delta_{\mathrm{c}} = 0.059\,\mathrm{nm}$ and $b = 0.25\,\mathrm{nm}$.

lie in the nonlinear portion of the $(T - \Delta)$ law the subsequent FEM solution is incorrect, leading to an incorrect solution for the total opening. When using realistic material properties $\delta_{\mathrm{c}} < b$, dislocation fields of order b, equivalent to the interaction of a single dislocation with the cohesive zone, can lead to failure of the superposition scheme. The use of adaptive time stepping and Newton–Raphson iterative schemes do not reliably resolve the issue even for time increments equal to 1×10^{-12} s. This behavior is illustrated in figure 3, where the upper plots show the dislocation displacement field ($\tilde{\Delta}$) along the crack line and the lower plots show the resulting crack opening profile obtained from the finite element solution, for two different snapshots in time of a DD/CZ simulation. The solution from the standard superposition is initially smooth (figure 3(*a*)) when $\tilde{\Delta} < b$ but as $\tilde{\Delta}$ approaches b (figure 3(*b*)) the numerical solution displays incorrect and extreme oscillatory behavior, illustrating failure of the standard superposition scheme.

To avoid the above problem, which is fundamentally a failure of the superposition method applied to a nonlinear cohesive zone we use the alternative superposition scheme of [35] shown schematically in figure 4. The [35] method is similar in spirit to the Eshelby inclusion problem [36]. Briefly, two problems are solved: (a) a standard DD problem in the domain where DD plasticity is permitted, but subjected to zero displacement boundary conditions independent of the actual boundary conditions (figure 4); and (b) an elastic/cohesive zone problem of the entire domain without dislocations, with all the desired loading and boundary conditions, and including the negative of the computed boundary tractions of problem (a) (figure 4). The superposition of problems (a) and (b) then yields the exact solution of the posed boundary value problem. Problem (a) is solved using the standard DD methodology but with the special boundary conditions while problem (b) is solved using standard finite element methodology with a Newton–Raphson (NR) iterative scheme to accurately capture the nonlinearity of the cohesive zone model. In this approach, superposition is applied only *within* the DD domain and not along its boundaries. The cohesive zone thus lies *outside* the domain of superposition. Dislocation interactions with the cohesive zone are captured through the tractions developed in the (a) that are imposed on the cohesive zone in problem (b). Thus

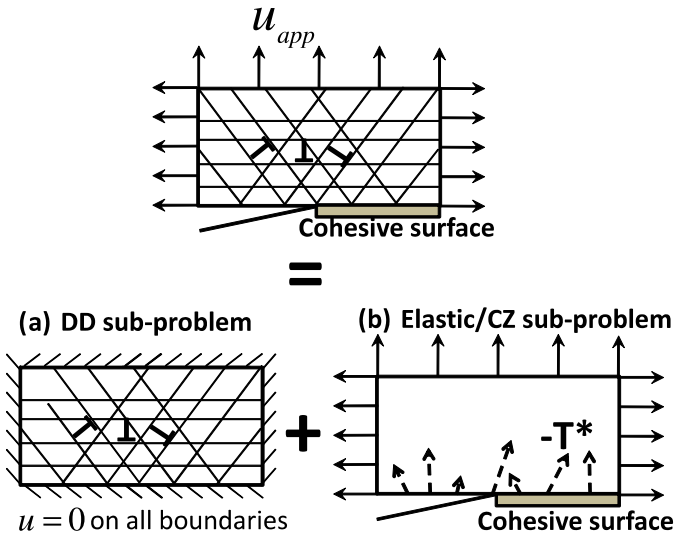

Figure 4. Schematic decomposition of the fracture problem using the alternative superposition scheme of [35].

the incremental statement of virtual work for the elastic/CZ problem (b) can now be written as

$$\int_V \hat{\sigma}\,\delta\epsilon\,\mathrm{d}V + \frac{1}{2}\int_{S_{\mathrm{coh}}} K(\hat{\Delta}^t)\hat{\Delta}\delta\Delta\,\mathrm{d}S = \frac{1}{\Delta t}\left\{\int_V \hat{\sigma}^t\delta\epsilon\,\mathrm{d}V - \frac{1}{2}\int_{S_{\mathrm{coh}}}\left[T(\hat{\Delta}^t) + T^*\right]\delta\Delta\,\mathrm{d}S\right\}, \tag{7}$$

where T^* are the tractions obtained on the boundary from the solution of problem (a). Transmission of dislocations into the cohesive zone can still occur, thereby opening the cohesive zone as should occur physically, but without spurious instabilities due to an inappropriate use of superposition. Figure 3 shows that instabilities reported with the standard superposition are eliminated with the use of alternate superposition. We note that this problem does not necessarily arise in most prior DD simulations, where $\sigma_{\mathrm{coh}} \leqslant 1$ GPa and $\delta_{\mathrm{c}} \gg b$.

6. Moving mesh method

For any problem involving a cohesive zone model, a finite element mesh must resolve the high stresses and stress gradients in the vicinity of the crack tip as it moves. The minimum element size near the crack tip is $\sim\delta_{\mathrm{coh}}/3$, as determined via numerical studies. For realistic cohesive zone properties, $\delta_{\mathrm{c}} \sim 0.1$ nm and $\delta_{\mathrm{coh}} \sim 1$ nm, requiring a mesh on the Å scale. At the same time, fracture toughness in the presence of plasticity is achieved only after significant (1–100 μm) crack growth and development of a plastic wake. Capturing micrometers of crack growth with sub-Å mesh sizes requires innovative computational methods; a simple uniform sub-Å mesh extending over micrometers of material is computationally intractable. Previous DD studies have thus used lower cohesive strengths, corresponding to $\delta_{\mathrm{coh}} > 100$ nm and much larger mesh sizes, and even then have not always investigated crack growth sufficient to establish the entire resistance curve.

Standard adaptive meshing methods involve re-meshing, which requires costly decomposition of the stiffness matrix with every re-meshing operation. For elasticity problems

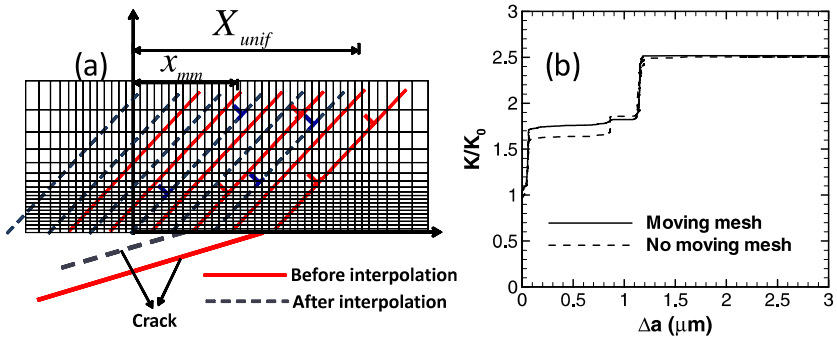

Figure 5. (*a*) Schematic of the moving mesh method, showing the backward translation of all slip planes, dislocations and field quantities, including crack plane displacements, after the crack has grown forward by some small amount. (*b*) Stress intensity versus crack growth, as computed using the moving mesh method (solid line) with $\Delta X_{\text{unif}} = 35\delta_{\text{coh}} = 1.1\,\mu\text{m}$, $x_{\text{mm}} = 20\delta_{\text{coh}}$ and a fixed mesh of the same fine-scale resolution (dashed line), $\Delta X_{\text{unif}} = 4\,\mu\text{m}$, $x_{\text{mm}} = 4\,\mu\text{m}$. Material properties are $\Gamma_0 = 1.1\,\text{J m}^{-2}$, $\sigma_{\text{coh}} = 1\,\text{GPa}$ and $\sigma_{\text{Y}} = 200\,\text{MPa}$, giving $\delta_{\text{coh}} = 32\,\text{nm}$.

such as the DD corrective solution, this can be avoided using what we term the 'moving mesh' method. The essence of this method is that, in a frame of reference moving with the crack tip, the dislocations, and all field variables including those of the cohesive zone, can be considered as moving in the opposite direction. The moving mesh method allows the crack to grow forward for some distance and then shifts the dislocations and field variables backward by exactly that amount, thus re-establishing the crack tip at the original location relative to the original mesh, leaving the stiffness matrix unchanged. A more detailed description is given below.

A uniform mesh of size $\Delta x_{\text{unif}} = \delta_{\text{coh}}/4$, suitable for resolving the cohesive zone, is placed around the initial crack tip and extending a distance X_{unif} ahead of the crack tip. Further away, the mesh size increases smoothly with increasing distance from the crack tip. During loading, the crack tip position is monitored at each increment. If the crack tip position passes a preselected distance x_{mm}, which is an even integer multiple of Δx_{unif}, then all finite element field quantities (stresses, strains and displacements) are interpolated from any nodal position x to the nodal position $x - x_{\text{mm}}/2$. All dislocation slip planes are also moved from positions x_{slip} to positions $x_{\text{slip}} - x_{\text{mm}}/2$. Figure 5(*a*) shows a typical near-tip mesh and schematic of the interpolation process. With x_{mm} and X_{unif} integer multiples of Δx_{unif}, the interpolation in the uniform mesh region around the crack tip is *exact* and is equivalent to transferring field quantities from a nodal position i to a position $i - N_{\text{mm}}$, where $N_{\text{mm}} = \text{int}(x_{\text{mm}}/2\Delta x_{\text{unif}})$. Small errors associated with the interpolation of field quantities and evaluation of dislocation stresses outside the uniform mesh region are then eliminated by performing a new corrective field solution with all dislocations fixed at the new positions. Since the mesh remains fixed, the stiffness matrix remains unchanged during this process. The method ensures that the crack tip is always located between 0 and x_{mm} and thus in the regime of full resolution for the cohesive zone.

The extent of the uniform mesh ahead of the crack tip determines the accuracy of the solution. Numerical studies over the parameter range $X_{\text{unif}} = 10\delta_{\text{coh}}$ to $50\delta_{\text{coh}}$ with $x_{\text{mm}} \approx X_{\text{unif}}/2$ show that $X_{\text{unif}} = 20\delta_{\text{coh}}$ is sufficient to produce mesh independent results. Figure 5(*b*) shows the crack resistance curve as calculated using the moving mesh method and using a mesh of the same fine-scale resolution but extending over the entire length of the crack growth shown. The results are essentially identical because the precise evolution of the

dislocation system and crack growth are sensitive to round-off errors (reflecting the chaotic aspects of dislocation dynamics) [37], so that small differences due to the meshing away from the crack tip region modify the detailed crack growth process.

7. Modeling of crack growth

Here we demonstrate that the collective set of algorithms described above permit for the stable calculation of extensive crack growth in a material with both high yield stress and high cohesive strength. Prior to that demonstration, we comment on other developments that are pertinent to DD modeling of plastic flow and fracture.

First, we have recently shown that the DD material properties can be tuned to obtain a desired yield stress [38]. An analytic model based on the traditional source/obstacle pileup model predicts a yield stress of

$$\sigma_{\mathrm{Y}} = \frac{1}{S}\sqrt{\frac{4\mu b}{\pi(1-\nu)}\frac{\tau_{\mathrm{obs}}}{1.5L_{\mathrm{obs}}} + \tau_{\mathrm{s}}^2}, \tag{8}$$

where L_{obs} is the average obstacle spacing in a system with maximum obstacle spacing of $1.5L_{\mathrm{obs}}$ and S is the Schmid factor. The high accuracy of this formula has been demonstrated by direct DD simulations for both single source/obstacle configurations and full tension specimens. Those DD studies required use of both the velocity correction and the modified nucleation criterion.

Second, in all DD calculations of the type discussed here, a major fraction of the computational effort is devoted to computing the dislocation-dislocation interactions, the dislocation-boundary corrections, and the source nucleation. As the total number N of dislocations in the computational cell increases, the incremental computational effort using direct methods scales as N^2 and the total effort scales as N^3. To reduce the computational burden significantly, we have implemented the FMM [39] which reduces the computational effort to $O(N)$, and has previously been applied to 2D DD simulations [40]. When applied to dislocation–dislocation interactions, the dislocation-boundary corrections and the source nucleation the total solution time per iteration in 2D-DD simulations is $O(N_{\mathrm{d}} + N_{\mathrm{s}} + N_{\mathrm{B}})$ where N_{d} is the number of dislocations, N_{s} is the number of sources and N_{B} is the number of boundary points. Our FMM implementation is based on the expansion of expressions for the displacements and stresses in terms of complex potentials [40, 41]. For deformation problems (bending, tension, etc), complex potentials for the field of a dislocation in an infinite medium are used. For problems involving a crack, where the resolution of the traction free crack surface near the crack tip is of critical importance in establishing conditions for crack growth, complex potentials for dislocations in a semi-infinite half-space are used. The FMM procedure using the infinite or half-space potentials is not significantly different from [40] and is not discussed here. FMM has tunable accuracy and we have found that eight digit accuracy ($\sim 10^{-8}$) for both displacements and stresses gives an excellent combination of speed and accuracy for use in 2D DD simulations. The velocity correction of (2) requires computation of the spatial derivative of the Peach–Koehler force along the slip plane, which involves computation of derivatives of the complex potentials. Evaluation of these derivatives can also be performed with computational effort of $O(N)$ in a very straightforward manner. Identifying that the derivatives of the dislocation stress fields decay as $1/r^2$, the computational effort in evaluating the derivatives can be further minimized by including the contribution of only 'close range' dislocations, a process natural within the FMM framework.

Employing all the computational enhancements implemented as described in this paper, figure 6 shows the fracture resistance curve of a simulation in which the material yield

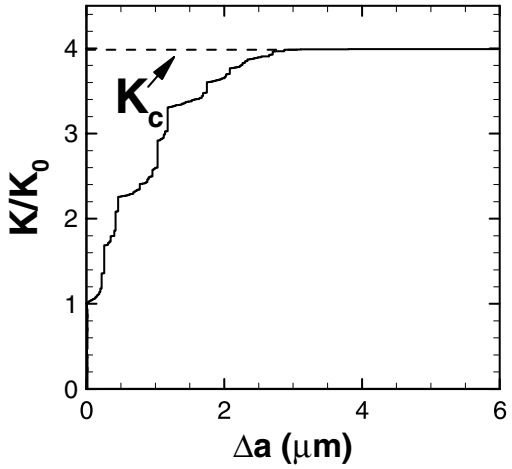

Figure 6. Stress intensity versus crack growth, showing stable growth of the crack with increasing load over several micrometers and culminating in a final fracture toughness K_c for a material with $\sigma_{coh} = 7\,\text{GPa}$, $\Gamma_0 = 1.1\,\text{J m}^{-2}$ and $\sigma_Y = 700\,\text{MPa}$, giving $\delta_c = 0.059\,\text{nm}$, $\delta_{coh} = 1.6\,\text{nm}$. Meshing scales are $\Delta x_{unif} = \delta_{coh}/4$, $X_{unif} = 35\delta_{coh}$, $x_{mm} = 20\delta_{coh}$.

stress is $\sigma_Y = 700\,\text{MPa}$, the cohesive strength is $\sigma_{coh} = 7\,\text{GPa}$, and the cohesive energy is $\Gamma_0 = 1.13\,\text{J m}^{-2}$, with $\delta_{coh} = 1.6\,\text{nm}$ and finesh mesh size $\Delta x_{unif} = 0.4\,\text{nm}$. Other parameters in the model are a Burgers vector $b = 0.25\,\text{nm}$, slip plane spacing $d = 100b$, areal density of sources $\rho_s = 66\,\mu\,\text{m}^{-2}$ with average source strength $\tau_s = 50\,\text{MPa}$, and an average obstacle spacing $L_{obs} = 3/\rho_{obs}d = 80\,\text{nm}$. Figure 6 shows that crack growth starts around the elastic value K_0, but dislocation activity dissipates energy and stabilizes crack growth. At a critical load K_c, plastic dissipation is insufficient to prevent crack growth and the crack grows with no further increase in load in a brittle manner. It can be seen that $3.2\,\mu\text{m}$ of crack growth is needed to establish K_c and no numerical instabilities or convergence issues are observed, even when the crack grows in the a brittle-like fashion after reaching K_c.

8. Summary

In summary, we have implemented several improvements to the existing 2D-DD/CZ methodology that significantly improve the capability to model materials with realistic material properties. These enhancements are

1. A gradient correction in the computation of the dislocation velocity that completely eliminates instabilities and oscillations in the standard forward-Euler approach and also eliminates the need for both an artificial dislocation cut-off velocity and an underrelaxation procedures present in earlier DD implementations.
2. Modified dislocation nucleation algorithm where the burger's vector and position of the 'latent' dislocation dipole varies linearly with the nucleation time, eliminating spurious jumps in the boundary displacements and stresses.
3. Use of the O'day and Curtin [35] superposition scheme to correctly capture dislocation interactions with the nonlinear cohesive zone that eliminates instabilities in problems with large (realistic) cohesive strengths.
4. A 'moving mesh method' to capture *a priori* arbitrary amounts of crack growth while retaining the required fine mesh resolution near the crack tip, which is achieved with almost no additional computational cost.

References

[1] Devincre B and Kubin L 1997 Mesoscopic simulations of dislocations and plasticity *Mater. Sci. Eng.* A **234–23** 8–14

[2] Kubin L, Devincre B and Tang M 1998 Mesoscopic modelling and simulation of plasticity in fcc and bcc crystals: dislocation intersections and mobility *J. Comput.-Aided Mater. Des.* **5** 31–54

[3] Hartmaier A, Fivel M, Canova G and Gumbsch P 1998 3D discrete dislocation models of thin-film plasticity *Proc. Materials Research Society Symp. (Boston, MA, USA)* vol 505, pp 539–44

[4] Fivel M C and Canova G R 1999 Developing rigorous boundary conditions to simulations of discrete dislocation dynamics *Modelling Simul. Mater. Sci. Eng.* **7** 753–68

[5] Devincre B, Kubin L, Lemarchand C and Madec R 2001 Mesoscopic simulations of plastic deformation *Mater. Sci. Eng.* A **309–310** 211–9

[6] Madec R, Devincre B and Kubin L P 2002 From dislocation junctions to forest hardening *Phys. Rev. Lett.* **89** 255–68

[7] Bulatov V, Cai W, Fier J, Hiratani M, Hommes G, Pierce T, Tang M, Rhee M, Yates K and Arsenlis T 2004 Scalable line dynamics in ParaDiS *SC '04: Proc. 2004 ACM/IEEE Conf. on Supercomputing (Washington, DC, USA)* pp 367–78

[8] Cai W, Bulatov V, Pierce T, Hiratani M, Rhee M, Bartlet M and Tang M 2004 Massively-parallel dislocation dynamics simulations *Solid Mechanics and Its Applications* vol 115 (Dordrecht: Kluwer)

[9] Wang M, Srolovitz D, Rickman J and Lesar R 2000 Dislocation motion in the presence of diffusing solutes: a computer simulation study *Acta Mater.* **48** 2163–75

[10] Shin C, Fivel M and Oh K 2001 Nucleation and propagation of dislocations near a precipitate using 3D discrete dislocation dynamics simulations *Journal De Physique. IV* **11** 527–34

[11] Shin C, Fivel M, Verdier M and Oh K 2003 Dislocation-impenetrable precipitate interaction: a three-dimensional discrete dislocation dynamics analysis *Phil. Mag.* **83** 3691–704

[12] Hiratani M and Zbib H M 2003 dislocation-defect interactions and patterning: stochastic discrete dislocation dynamics (SDD) *J. Nucl. Mater.* **323** 290–303

[13] Shin C, Fivel M, Verdier M and Robertson C 2005 Dislocation dynamics simulations of fatigue of precipitation-hardened materials *Mater. Sci. Eng.* A **400–401** 166–9

[14] Yashiro K, Kurose F, Nakashima Y, Kubo K, Tomita Y and Zbib H 2006 Discrete dislocation dynamics simulation of cutting of [gamma]' precipitate and interfacial dislocation network in Ni-based superalloys *Int. J. Plasticity* **22** 713–23

[15] Xiang Y and Srolovitz D 2006 Dislocation climb effects on particle bypass mechanisms *Phil. Mag.* **86** 3937–57

[16] Mastorakos I and Zbib H 2006 Shielding and amplification of a penny-shape crack due to the presence of dislocations *Int. J. Fract.* **142** 103–17

[17] Senger J, Weygand D, Gumbsch P and Kraft O 2008 Discrete dislocation simulations of the plasticity of micro-pillars under uniaxial loading *Scr. Mater.* **58** 587–90

[18] Motz C, Weygand D, Senger J and Gumbsch P 2008 Micro-bending tests: a comparison between three-dimensional discrete dislocation dynamics simulations and experiments *Acta Mater.* **56** 1942–55

[19] Weygand D, Poignant M, Gumbsch P and Kraft O 2008 Three-dimensional dislocation dynamics simulation of the influence of sample size on the stress-strain behavior of fcc single-crystalline pillars *Mater. Sci. Eng.* A **483–484** 188–90

[20] Van der Giessen E and Needleman A 1995 Discrete dislocation plasticity: a simple planar model *Model. Simul. Mater. Sci. Eng.* **3** 689–735

[21] Wang Z, Ghoniem N and LeSar R 2004 Multipole representation of the elastic field of dislocation ensembles *Phys. Rev.* B **69** 174102

[22] Wang Z, Ghoniem N, Swaminarayan S and LeSar R 2006 A parallel algorithm for 3D dislocation dynamics *J. Comput. Phys.* **219** 608–21

[23] Arsenlis A, Cai W, Tang M, Rhee M, Oppelstrup T, Hommes G, Pierce T G and Bulatov V V 2007 Enabling strain hardening simulations with dislocation dynamics *Modelling Simul. Mater. Sci. Eng.* **15** 553–95

[24] Deshpande V S, Needleman A and Van der Giessen E 2002 Discrete dislocation modeling of fatigue crack propagation *Acta Mater.* **50** 831–46

[25] O'Day M, Nath P and Curtin W 2006 Thin film delamination: a discrete dislocation analysis *J. Mech. Phys. Solids* **54** 2214–34

[26] Broedling N, Hartmaier A and Gao H 2006 A combined dislocation cohesive zone model for fracture in a confined ductile layer *Int. J. Fract.* **140** 169–81

[27] Broedling N C, Hartmaier A and Gao H 2008 Fracture toughness of layered structures: embrittlement due to confinement of plasticity *Eng. Fracture Mech.* **75** 3743–54

[28] O'Day M and Curtin W 2005 Bimaterial interface fracture: a discrete dislocation model *J. Mech. Phys. Solids* **53** 359–82
[29] Chakravarthy S and Curtin W 2010 Origin of plasticity length-scale effects in fracture *Phys. Rev. Lett.* **105** 115502
[30] Cleveringa H H M, Van der Giessen E and Needleman A 1999 A discrete dislocation analysis of bending *Int. J. Plasticity* **15** 837–68
[31] Deshpande V S, Needleman A and Van der Giessen E 2003 Discrete dislocation plasticity modeling of short cracks in single crystals *Acta Mater.* **51** 1–15
[32] Segurado J, Llorca J and Romero I 2007 Computational issues in the simulation of two-dimensional discrete dislocation mechanics *Model. Simul. Mater. Sci. Eng.* **15** 361–75
[33] Eshelby J D and Bilby B A 1968 *Fracture* vol I (New York: Academic) chapter 2
[34] Olmsted D L, Hector L G Jr, Curtin W and Clifton R 2005 Atomistic simulations of dislocation mobility in Al, Ni and Al/Mg alloys *Model. Simul. Mater. Sci. Eng.* **13** 371–88
[35] O'Day M P and Curtin W A 2004 A superposition framework for discrete dislocation plasticity *J. Appl. Mech.* **71** 805–15
[36] Eshelby J D 1961 Elastic inclusions and inhomegeneities *Progress in Solid Mechanics* vol ii ed I Sneddon and R Hill (Amsterdam: North Holland)
[37] Deshpande V S, Needleman A and Van der Giessen E 2001 Dislocation dynamics is chaotic *Scr. Mater.* **45** 1047–53
[38] Chakravarthy S and Curtin W 2010 Effect of source and obstacle strengths on yield stress: a discrete dislocation study *J. Mech. Phys. Solids* **58** 625–35
[39] Greengard L and Rokhlin V 1987 A fast algorithm for particle simulations *J. Comput. Phys.* **73** 325–48
[40] Jonsson A 2003 Discrete dislocation dynamics by an O(N) algorithm *Comput. Mater. Sci.* **27** 271–88
[41] Muskhelishvili N I 1963 *Some Basic Problems of the Mathematical Theory of Elasticity; Fundamental Equations, Plane Theory of Elasticity, Torsion, and Bending* (Groningen: Noordhoff)